Final Technical Report

Title of award

Using GPS to Measure the Slip Rate of the Honey Lake Fault, California

USGS Award Number:

G11AP20023

Principal Investigators:

William C. Hammond and Cornelis Kreemer

Contact Information:

Nevada Bureau of Mines and Geology
University of Nevada, Reno
1664 N. Virginia Street, Reno, NV 89557
Tel: 775-784-6436; Fax: 775-784-1709
Email: whammond@unr.edu

Term covered by the report:
January 1, 2011 to December 31, 2012

Using GPS to estimate slip rates of the Honey Lake/Warm Springs and Mohawk Valley fault zones, Northern Walker Lane

Jayne M. Bormann, William C. Hammond, Corné Kreemer, and Geoffrey Blewitt
Nevada Geodetic Laboratory
Nevada Bureau of Mines and Geology
University of Nevada, Reno

Abstract

We present new data from the semi-continuous Mobile Array of GPS for Nevada Transtension (MAGNET), continuous EarthScope Plate Boundary Observatory (PBO) and other GPS networks to measure contemporary slip rates on the Honey Lake and Mohawk Valley fault zones in northern California. We use an elastic block model to estimate kinematically consistent fault slip and block rotation rates from the GPS and geologic data, and compare the results to the small but growing database of geologic data on slip rates in the northern Walker Lane Belt. The GPS velocity field shows shear deformation of ~7 mm/yr across the northern Walker Lane, of which between 3.5-4 mm/yr is expressed as dextral shear deformation across these fault zones. Slip rates are estimated to be 2.2±0.2 mm/yr for Mohawk Valley and 1.1±0.2 mm/yr for Honey Lake faults. Model tests for slip on the Grizzly Valley fault, a structure sub-parallel to the other systems that is less developed geomorphically but is optimally oriented to accommodate the measured tectonic strain accumulation, find that a rate of 0.5 mm/yr or less could be allowed by the geologic and geodetic data. In all our models that fit the GPS data the Mohawk Valley fault consistently accommodates ~1 mm/yr more slip than the Honey Lake fault. The block models indicate a transition from transtensional oblique slip across faults near the latitude of Lake Tahoe in the central Walker Lane, to segregated dextral shear and normal extension in the most northern Walker Lane Belt.

Introduction

The Northern Walker Lane (NWL) is the northern segment of a ~100 km wide zone of intracontinental transtensional faulting that separates the northwest translating Sierra Nevada/Great Valley (SNGV) microplate from the extending Basin and Range province [*Stewart*, 1988; *Wesnousky*, 2005], and acts as an integral part of the Pacific/North American diffuse plate boundary zone (Figure 1). Geodetic studies indicate that up to 25% of the relative dextral motion between the Pacific and North American plates is accommodated east of the Sierra Nevada, with the majority of the deformation occurring in the Walker Lane and Eastern California Shear Zone. The amount of shear deformation in the Walker Lane decreases northward from ~10-12 mm/yr in the Southern Walker Lane [*Dixon et al.*, 2000; *Bennett et al.*, 2003] to ~7 mm/yr in the NWL [*Hammond and Thatcher*, 2007; *Hammond et al.*, 2011; *Wesnousky et al.*, 2012]. Active deformation is expressed as northwest striking, left-stepping, en-echelon dextral faults: the Pyramid Lake, Warm Springs Valley, Honey Lake, Grizzly Valley, and Mohawk Valley fault zones (Figure 1). Since the onset of strike-slip faulting between 3.5-3 Ma, these faults have accommodated ~20-25 km of cumulative dextral displacement [*Henry et*

al., 2007; *Faulds and Henry*, 2008]. Dividing the total displacement by the age of strike-slip initiation results in a long-term average deformation rate that is consistent with geodetic measurements of contemporary deformation across the shear zone [*Faulds and Henry*, 2008; *Hammond et al.*, 2011].

This study focuses on the most northwestern portion of the NWL, where the fault system is comprised by the relatively simple and sub-parallel Honey Lake, Grizzly Valley, and Mohawk Valley faults. The active trace of the Honey Lake fault is a northwest-striking single strand of fault scarps and tonal lineaments that extend for >50 km separating the Diamond Mountains to the west from the Honey Lake basin to the east [*Wills and Borchardt*, 1993]. The fault has accommodated ~5-10 km of total dextral displacement [*Faulds et al.*, 2005; *Henry et al.*, 2007]. Located approximately 50 km to the southwest of the Honey Lake fault, the Mohawk Valley fault zone strikes to the northwest for ~80 km along the eastern margin of the Sierra Nevada mountains. Deformation on the Mohawk Valley fault is partitioned between distributed zones of normal faulting along the western margin of the valley and a more active zone of dextral faulting along the eastern valley margin [*Sawyer et al.*, 2005]. Between the Honey Lake and Mohawk Valley fault systems lies the ~50 km long subparallel Grizzly Valley fault zone. The fault offsets glacial and alluvial fan deposits and the geomorphic expression is consistent with dextral strike-slip faulting [*Hitchcock et al.*, 2012]. Dextral offset across the structure is minimal [*Faulds and Henry*, 2008]. Recent geologic studies indicate that the Grizzly Valley fault has accommodated Quaternary dextral slip [*Gold et al.*, 2012; *Hitchcock et al.*, 2012].

Previous geodetic studies measuring contemporary deformation in the NWL find the highest rates of strain accumulation centered over the Mohawk Valley fault [*Dixon et al.*, 2000; *Hammond and Thatcher*, 2007; *Hammond et al.*, 2011]. Hammond *et al.* [2011] used GPS data to estimate dextral slip rates of 1.2 mm/yr for the Honey Lake fault zone and 2.9 mm/yr for the Mohawk Valley fault zone as part of a regional study of Northern Walker Lane deformation (Table 1). Although the range of geologically estimated slip rates (1.1-2.6 mm/yr) agrees to within uncertainties with the geodetically estimated slip rate for the Honey Lake fault, the geologic and geodetic estimates for the Mohawk Valley slip rate differ by a factor of 10. The high rates of strain accumulation measured across the Mohawk Valley fault are not completely unexpected as it experiences unusually high rates of microseismicity in comparison to other NWL faults [*Rogers et al.*, 1991; *Goter et al.*, 1994; *Kreemer and Hammond*, 2010; Figure 2]. More than 30 M>4 earthquakes have occurred in the vicinity of the Mohawk Valley fault since 1960, with the largest event being the 2001 M_w 5.2 Portola Earthquake [Nevada Seismological Laboratory Catalog; *Kreemer and Hammond*, 2010]. From August 2011-June 2012, a ~30 km deep earthquake sequence resulted in more that 2200 earthquakes of M<1.9 beneath the southern portion of Mohawk Valley fault. An M_L 4.9 earthquake occurred at 12 km depth near the swarm on October 29, 2011 is likely related to stress changes induced by the deeper activity. Focal mechanisms for earthquakes along the Mohawk Valley fault zone are predominately strike-slip with one nodal plane oriented to the NW, indicating compatibility with dextral shear [*Ichinose et al.*, 2003; *Kreemer and Hammond*, 2010].

We present new data from the semi-continuous Mobile Array of GPS for Nevada Transtension (MAGNET) [*Blewitt et al.*, 2009] in complement with continuous GPS data from the EarthScope Plate Boundary Observatory (PBO) and other GPS networks to measure contemporary deformation across the Honey Lake and Mohawk Valley fault zones. We use an elastic block model to estimate kinematically consistent fault slip and block rotation rates from the GPS data. Slip rates estimated from geodetic measurements are dependent on model

assumptions, the effects of which are not necessarily represented in formal inversion uncertainties. Geodetic measurements place strong constraints on slip rate budgets across systems comprised of multiple faults, allowing for some covariance between slip rate estimates on the near-parallel systems such as the Honey Lake and Mohawk Valley fault zones. The block model allows us to constrain the uncertainties in slip rates on both systems and provide realistic estimates of slip rate uncertainties by testing (1) the effects of block geometry assumptions on estimated fault slip rates, (2) the range of slip rates permissible by the GPS data, and (3) slip rate covariance between neighboring faults.

GPS Data

We analyze GPS data from 111 semi-continuous and continuous sites in the NWL and SNGV microplate to produce a horizontal velocity field that describes present-day deformation across the Honey Lake and Mohawk Valley fault systems (Figure 3). The flexibility and efficiency of the semi-continuous MAGNET occupation strategy allows us to maintain a dense GPS network with 10-20 km average station spacing throughout the NWL [*Blewitt et al*., 2009]. Initial MAGNET occupations began in 2004, and the network continues to evolve and expand. In the NWL, MAGNET stations have at minimum 3-4 years of data collected in at least 3 different month-long occupations. We supplement MAGNET data with GPS data from the PBO, BARGEN and BARD continuous networks available through the UNAVCO data archive. The longest running continuous sites have time series lengths of more than 10 years and most PBO sites have at least 4-5 years of data available. In this analysis, we include data collected through August 2012 from semi-continuous and continuous sites with a time series length of greater than 3 years.

The GPS coordinate time series used in this study were derived as part of a global solution that includes over 10,000 stations. The daily station coordinates were estimated using the precise point position method [*Zumberge et al.*, 1997] of the GIPSY-OASIS II software package from the Jet Propulsion Laboratory (JPL). The processing utilizes reanalyzed fiducial-free GPS satellite orbit and clock parameters provided by JPL. The observation model includes solid earth tides and oceanic tidal loading, tropospheric delay modeled as a zenith parameter with two random walk gradient parameters, antenna calibration models for station receivers and satellite transmitters, and station clock biases estimated as a white noise process. Carrier phase ambiguities are resolved using the Ambizap3 software [*Blewitt*, 2008] to produce a globally-consistent solution with full network resolution better than 1 mm.

We align the daily position solutions with a custom North America-fixed reference frame, NA12 [*Blewitt et al.*, 2012]. NA12 is a derivative frame of IGS08, the GPS based realization of the International Terrestrial Reference Frame (ITRF2008). The frame is composed of 300 stations distributed throughout North America and a core subset of 30 stations selected to impose the no-net rotation constraint that minimizes the horizontal velocities of points within geographically stable North America (regions not affected by plate boundary deformation or postglacial isostatic adjustment). The resulting frame co-rotates with stable North America, is spatially filtered to remove continental scale common mode errors, and is tied to JPL's daily realization of IGS08. NA12 coordinate time series have RMS residuals of 1.0, 0.9, and 3.4 mm/yr in the north, east, and vertical directions, respectively [*Blewitt et al.*, 2012]. The seven parameter daily coordinate transformations from IGS08 to NA12 are publicly available for GIPSY-OASIS II users at ftp://gneiss.nbmg.unr.edu/xfiles.

In order to use GPS data to infer long-term patterns and rates of deformation from an elastic block model, the position time series must be free of non-linear, transient motions. Large earthquakes may affect GPS station position initially with permanent co-seismic displacements that can be followed by transient perturbations to secular station motion resulting from frictional afterslip on the fault plane, poroelastic rebound of fluids in the upper crust, or viscoelastic relaxation in the lower crust and upper mantle [e.g. *Pollitz*, 1997; *Feigl and Thatcher*, 2006; *Bürgmann and Dresen*, 2008]. Whereas transient motion due to afterslip and poroelastic rebound decays in the weeks to months following an earthquake [*Feigl and Thatcher*, 2006], postseismic deformation from viscoelastic relaxation can affect locations hundreds of kilometers from the earthquake source for years to decades following the event [e.g. *Gourmelen and Amelung*, 2005; *Freed et al.*, 2007; *Pollitz et al.*, 2008; *Hammond et al.*, 2009; 2010]. The NWL is located between 50-150 km west of a band of seven historic surface rupturing earthquakes (M 6.3-7.6) that occurred between 1915-1954, called the Central Nevada Seismic Belt (CNSB). Previous geodetic studies [*Hetland*, 2003; *Gourmelen and Amelung*, 2005; *Hammond et al.*, 2009] find evidence that transient deformation due to viscoelastic relaxation following the CNSB earthquakes affects GPS measurements in the NWL. We use the method of Hammond *et al.* [2010] to correct the GPS position time series using the preferred western Basin and Range viscosity structure determined by Hammond *et al.* [2009]. The Maxwell rheology viscoelastic model has a laterally homogeneous 15-km-thick elastic upper crust that overlies a 15-km-thick stronger lower crust ($\eta_{LC} = 10^{20.5}$ Pa·s) and weaker upper mantle ($\eta_{UM} = 10^{19}$ Pa·s). The relaxation response results from stress induced in the lower crust and upper mantle by sudden movement due to brittle failure of the upper crust. Initially, the stress is concentrated in the regions immediately surrounding the fault; however over time, the stress diffuses outwards and decays. The viscoelastic correction causes small (typically < 1 mm/yr) but non-zero changes in velocities throughout the study area.

We estimate interseismic station velocities from the corrected daily coordinate time series through a least squares inversion. For each station, we solve for the intercept b, velocity v, annual and semi-annual terms $\boldsymbol{C}_j$ and $\boldsymbol{S}_j$ for j = 1 and 2, and the size of previously identified steps in the coordinate time series $\boldsymbol{D}_k$:

$$x(t) = b + vt + \sum_{j=1,2} [\boldsymbol{C}_j \cos(j\omega t) + \boldsymbol{S}_j \sin(j\omega t)] + \sum_{k=1}^{M} [\boldsymbol{D}_k H(t - t_k)].$$

We estimate the rate v separately for the east, north, and vertical directions. The $\boldsymbol{D}_k$ terms are associated with discontinuities in continuous time series from known equipment or GPS system changes, coseismic offsets, or other non-geophysical effects that are not representative of secular tectonic deformation. The number M and timing t_k of these steps are identified for each individual component using the heuristic algorithms and selection criteria of Goldfarb *et al.* [2012] prior to applying the viscoelastic correction. Steps are not estimated for MAGNET time series because equipment in MAGNET is homogenous and is thought not to exhibit discontinuities from equipment changes. The annual and semi-annual terms may be poorly constrained for MAGNET stations with a sparse occupation history. To minimize this consequence, we damp the amplitude of seasonal terms using an *a priori* value of 0.5 mm/yr for all GPS stations.

We compute the uncertainty for each velocity as a combination of the formal rate uncertainty, which is a function of the daily position uncertainties, and additional uncertainty associated with the viscoelastic correction. To determine the uncertainty in the postseismic correction, we estimate the variance in velocities predicted by the set of viscoelastic models

determined by Hammond *et al.* [2009] to adequately fit the GPS and InSAR measured deformation in Central Nevada [after *Hammond et al.*, 2011]. We combine the formal uncertainty and the viscoelastic correction uncertainty using the square root of the sum of squares. For long-running stations that are far from the CNSB earthquakes, uncertainties estimated in this manner may still be unrealistically small, and so apply an uncertainty floor of 0.2 mm/yr in both the east and north directions. To control the quality of our interseismic velocity field, we eliminate stations that have horizontal velocity uncertainties greater than 2 mm/yr, stations with obviously outlying velocities or vertical velocities greater than 5 mm/yr as these measurements maybe influenced by anthropogenic or other non-tectonic geologic processes. Additionally we omit velocities from the MAGNET sites RENO, MOGL, and VRDE because the time series include coseismic offsets and afterslip resulting from the 2008 Mogul seismic swarm in west Reno [*Blewitt et al.*, 2008], and thus the calculated velocities are not representative of secular interseismic motion.

Velocities for GPS sites used in this study are presented in Figure 3. We estimate velocities for 85 MAGNET, 19 PBO, 4 BARD, and 3 BARGEN stations. 104 of the 111 GPS velocities are shown in Figure 2. We use the other 7 continuous stations (CHO1, ORBV, P140, P276, P310, P344, SUTB) to solve for the motion of the SNGV microplate [after *Hammond et al.*, 2011], which forms the western boundary condition for Walker Lane deformation. In Figure 3A we show the velocity field with respect to stable North America (NA12 frame) and in Figure 3B with respect to the SNGV microplate. Subtracting the motion of the SNGV microplate from the NA12 velocities highlights features in the velocity field near the western edge of the Walker Lane that are otherwise difficult to see.

The velocities presented with respect to stable North America are oriented to the northwest and increase from east to west across the NWL. We use a subset of these velocities (stations between the Pyramid Lake and Mohawk Valley faults) and the methods of Savage *et al*. [2001] to determine the azimuth of maximum shear strain is N45°W in the NWL. Figure 4 shows profiles of the velocity components parallel and perpendicular to this direction for a transect that crosses the Mohawk Valley, Grizzly Valley, and Honey Lake faults. Deformation across the transect is sub-parallel to the direction of Walker Lane shear and Pacific-North America relative plate motion, with a total velocity increase of ~6 mm/yr in the northwest direction and velocities <1 mm/yr perpendicular to the direction of shear. Shear deformation is concentrated across the northwest-striking dextral faults, where velocities in the northwest direction increase by ~4-5 mm/yr. Though the westward increase in velocity is visibly smooth, there is a recognizable change in slope in the N45˚W rate, perpendicular to the profile, near the site HONY and just east of the location of the Honey Lake Fault. The rate between HONY and the SNGV is ~4 mm/yr and is the budget across the most northwestern region of the NWL; although we note that block rotation and shear deformation result in velocity increases that are difficult to differentiate from a linear array of observations**,** and that both processes may contribute to the observed velocity increase in the NWL.

The profiles in Figure 4 show the velocities corrected for postseismic deformation (red circles with error bars) and the uncorrected corrected velocities (grey circles). The velocities changes are similar for sites across the study area, illustrating that the magnitude of the correction is small and is similar for all stations. Therefore, we infer that postseismic viscoelastic relaxation from the Central Nevada Seismic Belt earthquakes is not introducing transient gradients within the velocity field that could bias estimates of slip rates.

Fault Slip Rate Estimation

We use an elastic block model to estimate kinematically consistent long-term fault slip rates from our interseismic velocity field. Block modeling is a commonly used technique that relates block motions and fault slip rates to interseismic geodetic measurements [e.g. *Bennett et al.*, 1996; *Prawirodirdjo et al.*, 1997; *McCaffrey*, 2002; *Meade and Hager*, 2005; *Hammond and Thatcher*, 2007; *McCaffrey et al.*, 2007; *Meade and Loveless*, 2009] In this method, the study region is divided into a mosaic of contiguous, elastic, fault-bounded blocks based on the mapped traces of active faults. The block interfaces are locked at surface and slip only in earthquakes, but slip constantly at depth. In the interseismic period, strain accumulates smoothly and continuously across the medium surrounding the locked faults, however when averaged over many seismic cycles, the relative motion between blocks is a discontinuous step. The long-term block motion, approximated as a rigid block rotation on a sphere, is the sum of the velocities due to smooth interseismic strain accumulation and coseismic strain release,

$$v_{longterm} = v_{interseismic} + v_{coseismic} .$$

Elastic block models implement the "back slip" method of *Savage* [1983] to define interseismic GPS velocities as the sum of the rigid block motion minus the coseismic velocity

$$v_{interseismic} = v_{longterm} - v_{coseismic} .$$

The "coseismic velocity" or fault slip rate is defined as the average rate of motion of a point near a fault due to coseismic slip over many earthquake cycles with respect to a point on the other side of the fault. The strike-slip and dip-slip rates are modeled using unit slip functions [*Okada*, 1985] that represent patterns of surficial deformation due to slip on finite rectangular dislocations in the seismogenic crust.

We use the method of Hammond *et al.* [2011], which simultaneously solves for long-term block motion and the dip-slip and strike-slip components of fault slip rate through a regularized weighted least squares inversion. Our model is subject to regularization constraints that require consistency between relative block motions and fault slip rates and minimize fault slip rates and block centroid vertical axis rotations (spin rate). The model can solve for the uniform horizontal tensor strain rate for any block that has evidence of permanent internal deformation, and we can constrain slip rates and block rotations to match predetermined values. Our model does not solve for locking depth or fault dip, so we must assign these parameters for each solution.

The major northwest striking dextral faults in our study area are complimented by northerly striking normal faults and northeast striking sinistral faults that collectively accommodate Pacific/North American plate boundary deformation in a complex and diffuse fault network (Figure 1). We draw block boundaries first to coincide with the surface traces of major active faults (modified from fault sources in the 2008 National Seismic Hazard Maps [*Petersen et al.*, 2008] and the USGS Quaternary Fault and Fold database [*U.S. Geological Survey, California Geological Survey, and Nevada Bureau of Mines and Geology, 2006*] , and then connect these segments following the traces of minor faults, patterns of seismicity (data from the Advanced National Seismic System, *ANSS,* 2012), and major topographic features (Figure 3).

Our model is intended to rigorously estimate kinematically consistent slip rates on the major northwest-striking dextral faults in the NWL from GPS data. Models with too few blocks will concentrate slip from unmodeled faults onto the selected modeled faults, which may result in artificially increased slip rate estimates for the modeled faults. We have therefore strived to construct the model as completely as possible to accurately parameterize the deformation (Figure

2). In addition to deciding the location of block boundaries that represent faults in our model, we also must specify the dip and locking depth for each modeled fault segment. We assign dips of 80° for strike-slip faults and 45° for dip-slip faults [after *Hammond et al.*, 2011]. Where data is available, we use geologic studies or seismicity information to assign the dip direction for faults in our model. Where this information is not available, we infer the dip direction from topography. We assign a locking depth of 15 km for all faults in our model, which is generally considered the maximum depth of seismicity in the Basin and Range and is similar to the locking depths used in other block modeling studies in the western United States [e.g. *d'Alessio et al.*, 2005; *Meade and Hager*, 2005; *Spinler et al.*, 2010; *Hammond et al.*, 2011]. We hold the locking depth and fault dips constant in all tested models. We fix the motion of the SNGV microplate to match our previously determined rotation, thus maintaining a constant western boundary condition for all model variations.

We estimate the secular motion of 26 blocks and slip rates on 55 faults composed of 135 fault segments. Although geophysical models are inherently non-unique, we have certain prior expectations that help to discriminate between model solutions. Our first expectation is that adjacent faults of similar orientation will to respond to regional tectonic deformation with similar slip styles. Second, we expect deformation patterns to vary smoothly across the model region. We use two stochastic damping regularization parameters that minimize fault slip rates and block centroid vertical axis rotations to select solutions that fit the GPS data with smooth and simple models. Model regularization also allows us to include blocks that are not constrained by GPS data. Three out of 26 blocks in our model lack GPS velocities due to limitations in the density of GPS data coverage or difficulties measuring the movement of blocks that are largely covered by lakes. Although these blocks are small, they are clearly delineated by active faults suggesting independent block behavior. In the absence of GPS velocities, the motion of these blocks is averaged from the neighboring blocks. We select preferred values for the a priori uncertainty in the damping parameters through a grid search approach that finds a balance between model misfit and slip rate and spin rate norms [after *Hammond et al.*, 2011]. The model assumptions and regularization parameter variances are listed in Table 2.

Developing a block model that accurately represents the NWL fault network and connects these faults in a kinematically consistent manner is unavoidably subjective and is dependent on the modeler's assumptions. The effects of these assumptions on fault slip rates are difficult to quantify and are not represented in the formal inversion uncertainties. A known issue with modeling fault slip rates from GPS data is the covariance between slip rates on parallel-striking faults. Starting with a model that represents all faults allows us to test the effects of removing individual faults and combining blocks on the slip rates estimates for neighboring faults. To establish maximum slip rates on the Honey Lake and Mohawk Valley we first present the results of a model that does not include the sub-parallel Grizzly Valley fault. We then add the Grizzly Valley fault to the model to see what constraints the GPS data can put the Grizzly Valley slip rate and how the inclusion of an additional fault reduces slip rates on the Honey Lake and Mohawk Valley faults.

Results

The block model results illustrate the change in style of deformation from oblique extension on north-striking normal faults in Carson Valley, Tahoe Basin, and other valleys in the southern portion of the model to dextral shear on northwest-striking strike-slip faults in the NWL

(Figure 5). Slip predicted on the Mohawk Valley, Honey Lake, Warm Springs Valley, and Pyramid Lake faults is almost purely strike-slip, whereas normal motion with significant oblique slip is predicted on the West Tahoe Fault. These differences are a part of a general pattern of transition from dextral oblique normal slip in the southern part of the model to segregated fields of dextral shear in the northwest and normal extension in the northeast parts of the model.

Because the shear across the NWL varies smoothly and the shear is sub-parallel to the strike of the major faults (Figure 3), incorporating the Grizzly Valley fault (GVF) into the model strongly effects the slip rate predictions on the neighboring Mohawk Valley and Honey Lake faults. The model without the GVF (Figure 5) predicts dextral slip rates of 2.2 ± 0.2 mm/yr for the Mohawk Valley fault and 1.2 ± 0.2 mm/yr for the Honey Lake fault. Including the GVF reduces slip rates on the and Mohawk Valley and Honey Lake faults to 1.6 ± 0.2 mm/yr and 0.7 ± 0.2 mm/yr, respectively, and results in 1.4 ± 0.3 mm/yr of dextral slip on the GVF (Figure 6). The inclusion of the GVF does not appreciably change the sum of slip accommodated across the NWL; rather, the additional fault causes the slip to be distributed among 3 faults. Including the GVF results in a small but insignificant improvement to the model RMS residual velocities, which have an RMS of 0.5 (0.4) mm/yr in the north (east) components. We conclude that the geodetic data alone allows for up to ~1.5 mm/yr of dextral slip, but does not require any significant slip along the GVF. Furthermore, including the GVF does not alter the conclusion that the Mohawk Valley fault slips more rapidly that the Honey Lake fault.

Discussion

When summed, the geologically estimated slip rates on the Mohawk Valley and Honey Lake faults are in general agreement with the geodetically observed rate of deformation across the NWL [*Hammond et al.*, 2011], however slip rate discrepancies arise at the individual fault level. Previous geologic [*Wills and Borchardt*, 1993; *Sawyer et al.*, 2005; *Turner et al.*, 2008; *Gold*, 2012] and geodetic [*Hammond and Thatcher*, 2007; *Hammond et al.*, 2011] studies agree that these two faults collectively accommodate up to 3-4 mm/yr of dextral shear (Table 1), however the studies disagreed on the relative distribution of slip between the two fault systems. Geologic studies found that the Honey Lake fault zone is the major structure accommodating shear [*Wills and Borchardt*, 1993; *Turner et al.*, 2008; *Gold*, 2012], whereas geodetic studies indicate that the Mohawk Valley fault zone is the fastest slipping fault in the NWL [*Dixon et al.*, 2000; *Hammond and Thatcher*, 2007; *Kreemer and Hammond*, 2010; *Hammond et al.*, 2011].

As noted above, including the GVF in the inversion for slip rates reduces the slip rate on the Honey Lake fault to 0.7±0.2 mm/yr, without significantly damaging the fit to the GPS data. However, this rate is significantly lower than most of the geologically estimated rates (Table 1), and the geomorphic expression of the Honey Lake fault compared to the GVF indicates that it slips faster than the GVT [*Gold et al*, 2012]. Together these facts suggest that including the GVF in the inversion without constraint results in a GVF slip rate that is too high and a Honey Lake slip rate that is too low. We attempted to find a model that was consistent with geologic and geodetic data by imposing a slip rate of 1.0 mm/yr for the Honey Lake Fault, near the minimum permissible of the geologic rates from previous geologic studies (Table 1). This model has a GVF slip rate of 0.5 mm/yr, while not significantly changing the misfit to the GPS data. Assuming a larger slip rate for the Honey Lake fault that is still consistent with geologic

estimates would result in a smaller slip rate for the GVF. We conclude that the slip rate for the GVF is less than 0.5 mm/yr.

Conclusions

Our modeling shows that the Honey Lake, Grizzly Valley, and Mohawk Valley systems collectively accommodate ~3.5-4 mm/yr of shear deformation. Slip rates are estimated to be 2.2±0.2 mm/yr for Mohawk Valley and 1.1±0.2 mm/yr for Honey Lake faults. Regardless of modeling assumptions, the Mohawk Valley fault consistently accommodates ~1 mm/yr more slip than the Honey Lake fault and thus our results support the conclusion of previous work that the Mohawk Valley fault in the westernmost NWL is currently dominant in accommodating deformation in the NWL. Considering the geodetic data in along with past geologic studies suggest that the Grizzly Valley Fault has a slip rate of less than 0.5 mm/yr. Including the Grizzly Valley in our modeling does not alter the conclusion that the Mohawk Valley fault has a contemporary slip rate that is faster than the Honey Lake fault.

References for this Final Technical Report

Advanced National Seismic System, ANSS Worldwide Earthquake Catalog, accessed May 2011, from the Northern California Earthquake Data Center website: http://www.ncedc.org/anss/.

Bennett, R. A., W. Rodi, and R. E. Reilinger (1996), Global Positioning System constraints on fault slip rates in southern California and northern Baja, Mexico, *J. Geophys. Res*, *101*, 21,943–21,960.

Bennett, R., B. Wernicke, N. Niemi, A. Friedrich, and J. Davis (2003), Contemporary strain rates in the northern Basin and Range province from GPS data, *Tectonics*, *22*, 1,008.

Bennett, R. A., A. M. Friedrich, and K. P. Furlong (2004), Codependent histories of the San Andreas and San Jacinto fault zones from inversion of fault displacement rates, *Geol*, *32*, 961-964, doi:10.1130/G20806.1.

Blewitt, G. (2008), Fixed point theorems of GPS carrier phase ambiguity resolution and their application to massive network processing: Ambizap, *J. Geophys. Res*, *113*, B12410, doi:10.1029/2008JB005736.

Blewitt, G., J. Bell, W. C. Hammond, C. Kreemer, H. Plag, and C. dePolo (2008), GPS and InSAR Monitoring of the Mogul Swarm: Evidence for Mainly Aseismic Fault Creep, with Implications for Seismic Hazard, *Eos Trans. AGU, 89*(53), Fall Meet. Suppl. Abstract 53C-03.

Blewitt, G., W. C. Hammond, and C. Kreemer (2009), Geodetic observation of contemporary deformation in the northern Walker Lane: 1. Semipermanent GPS strategy, in *Late Cenozoic Structure and Evolution of the Great Basin – Sierra Nevada Transition*, edited by J. S. Oldow and P. Cashman, pp. 1-15, Geological Society of America Special Paper 447.

Blewitt, G., C. W. Kreemer, and J. M. Goldfarb (2012), Reference Frame NA12 for Studies of Continental Deformation in North America, *Abstract G51C-02 presented at 2012 Fall Meeting, AGU, San Francisco, Calif., 3-7 Dec*.

Bürgmann, R., and G. Dresen (2008), Rheology of the lower crust and upper mantle: Evidence from rock mechanics, geodesy, and field observations, *Annu. Rev. Earth Planet. Sci.*, *36*, 531.

d'Alessio, M., I. Johanson, R. Bürgmann, D. Schmidt, and M. Murray (2005), Slicing up the San Francisco Bay Area: Block kinematics and fault slip rates from GPS-derived surface velocities, *J. Geophys. Res*, *110*, B06403.

Dixon, T., E. Norabuena, and L. Hotaling (2003), Paleoseismology and Global Positioning System: Earthquake-cycle effects and geodetic versus geologic fault slip rates in the eastern California shear zone, *Geol*, *31*, 55-58.

Dixon, T., F. Farina, C. DeMets, and F. Suarez-Vidal (2000), New Kinematic models for Pacific-North America motion from 3 Ma to present, II: Evidence for a "Baja California shear zone", *Geophys. Res. Lett., 227*, 3961-3964.

Faulds, J. E. and C. D. Henry (2008), Tectonic influences on the spatial and temporal evolution of the Walker Lane: An incipient transform fault along the evolving Pacific–North American plate boundary, *Ores and orogenesis: Circum- Pacific tectonics, geologic evolution, and ore deposits*, edited by J.E. Spencer and S. R. Titley, Arizona Geological Society Digest *22*, pp. 437-470.

Faulds, J. E., C. D. Henry, and N. H. Hinz (2005), Kinematics of the northern Walker Lane: An incipient transform fault along the Pacific–North American plate boundary, *Geol*, *33*, 505-508, doi:10.1130/G21274.1.

Feigl, K., and W. Thatcher (2006), Geodetic observations of post-seismic transients in the context of the earthquake deformation cycle, *C. R. Geosciences*, *338*, 1012–1028.

Frankel, K. L., J. F. Dolan, L. A. Owen, P. Ganev, and R. C. Finkel (2011), Spatial and temporal constancy of seismic strain release along an evolving segment of the Pacific-North America plate boundary, *Earth and Planet. Sci. Lett., 304*, 565-576, doi:10.1016/j.epsl.2011.02.034.

Freed, A. M., R. Bürgmann, and T. Herring (2007), Far-reaching transient motions after Mojave earthquakes require broad mantle flow beneath a strong crust, *Geophys. Res. Lett.*, *34*, L19302, doi:10.1029/2007GL030959.

Friedrich, A., J. Lee, B. Wernicke, and K. Sieh (2004), Geologic context of geodetic data across a Basin and Range normal fault, Crescent Valley, Nevada, *Tectonics*, *23*, TC2015, doi:10.1029/2003TC001528.

Gold, R. D., R. W. Briggs, A. J. Crone, S., and Angster (2012), Honey Lake fault, Doyle, CA, in *Friends of the Pleistocene Pacific Cell Field Trip Guide Book, Neotectonics of the Lake Tahoe and Carson and Sierra Valleys*, edited by G. G. Seitz, September 13-16, 2012.

Gold, R. D., W. Stephenson, J. Odum, R. W. Briggs, A. J. Crone, and S. Angster (2012), Grizzly Valley fault system, Sierra Valley, CA, in *Friends of the Pleistocene Pacific Cell Field Trip Guide Book, Neotectonics of the Lake Tahoe and Carson and Sierra Valleys*, edited by G. G. Seitz, September 13-16, 2012.

Goldfarb, J., W. C. Hammond, G. Blewitt, and H.-P. Plag (2012), Automated Transient Identification and Characterization in GNSS Time Series, *abstract presented at 2012 UNAVCO Science Worksho*p.

Goter, S. K., D. H. Oppenheimer, J. J. Mori, M. K. Savage, and R. P. Masse (1994), Earthquakes in California and Nevada, Open-File Report 94-647, U.S. Geological Survey.

Gourmelen, N., and F. Amelung (2005), Postseismic mantle relaxation in the central Nevada seismic belt, *Science*, *310*, 1473-1476, doi:10.1126/science.1119798.

Gourmelen, N., T. H. Dixon, F. Amelung, and G. Schmalzle (2011), Acceleration and evolution of faults: An example from the Hunter Mountain–Panamint Valley fault zone, Eastern California, *Earth and Planet. Sci. Lett., 301*, 337–344, doi:10.1016/j.epsl.2010.11.016.

Hammond, W. C., and W. Thatcher (2007), Crustal deformation across the Sierra Nevada, northern Walker Lane, Basin and Range transition, western United States measured with GPS, 2000–2004, *J. Geophys. Res*, *112*, B05411, doi:10.1029/2006JB004625.

Hammond, W. C., C. Kreemer, and G. Blewitt (2009), Geodetic constraints on contemporary deformation in the northern Walker Lane: 3, Postseismic relaxation in the Central Nevada Seismic Belt, in *Late Cenozoic Structure and Evolution of the Great Basin – Sierra Nevada Transition*, edited by J. S. Oldow and P. Cashman, pp. 33-54, Geological Society of America Special Paper 447.

Hammond, W. C., C. Kreemer, G. Blewitt, and H.-P. Plag (2010), Effect of viscoelastic postseismic relaxation on estimates of interseismic crustal strain accumulation at Yucca Mountain, Nevada, *Geophys. Res. Lett.*, *37*, L06307, doi:10.1029/2010GL042795.

Hammond, W. C., G. Blewitt, and C. Kreemer (2011), Block modeling of crustal deformation of the northern Walker Lane and Basin and Range from GPS velocities, *J. Geophys. Res*, *116*, B04402, doi:10.1029/2010JB007817.

Henry, C. D., J. E. Faulds, and C. M. dePolo (2007), Geometry and timing of strike-slip and normal faults in the northern Walker Lane, northwestern Nevada and northeastern California: Strain partitioning or sequential extensional and strike-slip deformation?, in *Exhumation Associated with Continental Strike-Slip Fault Systems*, edited by A. B. Till et al., pp. 59-79

Geological Society of America Special Paper 434.
Hetland, E. A. (2003), Postseismic relaxation across the Central Nevada Seismic Belt, *J. Geophys. Res*, *108*, 2394, doi:10.1029/2002JB002257.
Hitchcock, C. S., D. F. Hoirup, B. G. Robbert, J. Pearce, and F. Glick (2012), LIDAR-based mapping of Late Quaternary faulting along the Grizzly Valley fault, Walker Lane Seismic Belt, California, *Abstract T51B-2558 presented at 2012 Fall Meeting, AGU, San Francisco, Calif., 3-7 Dec*.
Ichinose, G., J. Anderson, K. Smith, and Y. Zeng (2003), Source parameters of eastern California and western Nevada earthquakes from regional moment tensor inversion, *Bull. Seism. Soc. Am*, *93*(1), 61-84.
Kreemer, C. and W.C. Hammond (2010), Geodetic Constraints on the Slip Rate of the Mohawk Valley Fault Zone, California, Final Technical Report, United States Geological Survey NEHR, Award 08HQGR0027, 16 pp.
McCaffrey, R. (2002), Crustal block rotations and plate coupling, in *Plate Boundary Zones, Geodyn. Ser.*, vol. 30, edited by S. Stein and J. T. Freymueller, pp. 101–122, AGU, Washington, D. C., doi:10.1029/GD030p0101.
McCaffrey, R., A. I. Qamar, R. W. King, R. Wells, G. Khazaradze, C. A. Williams, C. W. Stevens, J. J. Vollick, and P. C. Zwick (2007), Fault locking, block rotation and crustal deformation in the Pacific Northwest, *Geophys. J. Int*, *169*, 1315–1340, doi:10.1111/j.1365-246X.2007.03371.x.
Meade, B. J., and J. P. Loveless (2009), Block Modeling with Connected Fault-Network Geometries and a Linear Elastic Coupling Estimator in Spherical Coordinates, *Bull. Seism. Soc. Am*, *99*(6), 3124–3139, doi:10.1785/0120090088.
Meade, B., and B. Hager (2005), Block models of crustal motion in southern California constrained by GPS measurements, *J. Geophys. Res*, *110*, B03403, doi:10.1029/2004JB003209.
Okada, Y. (1985), Surface deformation due to shear and tensile faults in a half-space, *Bull. Seism. Soc. Am*, *75*(4), 1135-1154.
Oskin, M., and A. Iriondo (2004), Large-magnitude transient strain accumulation on the Blackwater fault, Eastern California shear zone, *Geol*, *32*(4), 313-316, doi:10.1130/G20223.1.
Oskin, M., L. Perg, E. Shelef, M. Strane, E. Gurney, B. Singer, and X. Zhang (2008), Elevated shear zone loading rate during an earthquake cluster in eastern California, *Geol*, *36*(6), 507-510, doi:10.1130/G24814A.1.
Petersen, M. D., A. D. Frankel, S. C. Harmsen, C. S. Mueller, K. M. Haller, R. L. Wheeler, R. L. Wesson, Y. Zeng, O. S. Boyd, D. M. Perkins, N. Luco, E. H. Field, C. J. Willis, and K. S. Rukstales (2008), Documentation for the 2008 Update of the United States National Seismic Hazard Maps, 61 pp.
Pollitz, F. F. (1997), Gravitational-viscoelastic postseismic relaxation on a layered spherical Earth, *Journal of Geophysical Research*, *102*, 17,921-17,941.
Pollitz, F., P. McCrory, J. Svarc, and J. Murray (2008), Dislocation models of interseismic deformation in the western United States, *J. Geophys. Res*, *113*(B4), B04413.
Prawirodirdjo, L., Y. Bock, R. McCaffrey, J. Genrich, E. Calais, C. Stevens, S. Puntodewo, C. Subarya, J. Rais, and P. Zwick (1997), Geodetic observations of interseismic strain segmentation at the Sumatra subduction zone, *Geophys. Res. Lett.*, *24*, 2601–2604.
Richter, C. F., and B. Gutenberg (1956), Magnitude and energy of earthquakes, *Ann. Geof.,*

Roma, *9*, 1–15.
Rockwell, T. K., S. Lindvall, M. Herzberg, D. Murbach, T. Dawson, and G. Berger (2000), Paleoseismology of the Johnson Valley, Kickapoo, and Homestead Valley faults: Clustering of earthquakes in the eastern California shear zone, *Bull. Seism. Soc. Am*, *90*(5), 1200–1236.
Rogers, A. M., S. C. Harmsen, E. J. Corbett, K. Priestley, and D. dePolo (1991), The seismicity of Nevada and some adjacent parts of the Great Basin, in Neotectonics of North America: Geological Society of America, Decade Map Volume, edited by D. B. Slemmons, et al., pp. 153- 184.
Savage, J. C. (1983), A dislocation model of strain accumulation and release at a subduction zone, *J. Geophys. Res*, *88*(B6), 4984–4996.
Savage, J., W. Gan, and J. Svarc (2001), Strain accumulation and rotation in the Eastern California Shear Zone, *J. Geophys. Res*, *106*(B10), 21,995–22,007.
Sawyer, T. L., R. W. Briggs, and A. R. Ramelli (2003), Paleoseismic investigations of the Mohawk Valley fault zone, Sierra County, northeastern California, Annual Project Summary, U.S. Geological Survey National Earthquake Hazards Reduction Program, Award 04HQGR0089, 4 pp.
Sawyer, T. L., R. W. Briggs, and A. R. Ramelli (2005), Late Quaternary activity of the southern Mohawk Valley fault zone, northeastern California, *Seismol. Res. Lett.*, *76*, 248.
Schwartz, D. P., and K. J. Coppersmith (1984), Fault behavior and characteristic earthquakes: examples from the Wasatch and San Andreas fault zones, *J. Geophys. Res*, *89*(B7), 5681–5698.
Segall, P. (2002), Integrating geologic and geodetic estimates of slip rate on the San Andreas fault system, *International Geology Review*, *44*, 62-82.
Shelef, E., and M. Oskin (2010), Deformation processes adjacent to active faults: Examples from eastern California, *J. Geophys. Res*, *115*(B5), B05308, doi:10.1029/2009JB006289.
Spinler, J., R. Bennett, M. Anderson, S. McGill, S. Hreinsdóttir, and A. McCallister (2010), Present-day strain accumulation and slip rates associated with southern San Andreas and eastern California shear zone faults, *J. Geophys. Res*, *115*(B11), B11407, doi:10.1029/2010JB007424.
Stewart, J. H. (1988), Tectonics of the Walker Lane Belt, western Great Basin; Mesozoic and Cenozoic deformation in a zone of shear, paper presented at Rubey colloquium on Metamorphism and crustal evolution of the Western United States, Los Angeles, CA, 1988.
Thatcher, W. (2009), How the Continents Deform: The Evidence From Tectonic Geodesy, *Annu. Rev. Earth Planet. Sci.*, *37*(1), 237–262, doi:10.1146/annurev.earth.031208.100035.
Thatcher, W., G. R. Foulger, B. R. Julian, J. L. Svarc, E. Quilty, and G. W. Bawden (1999), Present-day deformation across the Basin and Range province, western United States, *Science*, *283*, 1714-1718.
Turner, R., R. D. Koehler, R. W. Briggs, and S. G. Wesnousky (2008), Paleoseismic and Slip-Rate Observations along the Honey Lake Fault Zone, Northeastern California, USA, *Bull. Seism. Soc. Am*, *98*(4), 1730–1736, doi:10.1785/0120070090.
U.S. Geological Survey (2006), California Geological Survey, and Nevada Bureau of Mines and Geology, Quaternary fault and fold database for the United States, accessed May 2012, from USGS web site: http://earthquakes.usgs.gov/regional/qfaults/.
Wesnousky, S. G. (2005), Active faulting in the Walker Lane, *Tectonics*, *24,* TC3009, doi:10.1029/2004TC001645.
Wesnousky, S. G., J. M. Bormann, C. Kreemer, W. C. Hammond, and J. N. Brune (2012),

Neotectonics, geodesy, and seismic hazard in the Northern Walker Lane of Western North America: Thirty kilometers of crustal shear and no strike-slip? *Earth and Planet. Sci. Lett., 329-330*(C), 133–140, doi:doi:10.1016/j.epsl.2012.02.018.

Wills, C. J., and G. Borchardt (1993), Holocene slip rate and earthquake recurrence on the Honey Lake fault zone, northeastern California, *Geology*, *21*, 853–856.

Zumberge, J. F., M. B. Heflin, D. C. Jefferson, M. M. Watkins, and F. H. Webb (1997), Precise point positioning for the efficient and robust analysis of GPS data from large networks, *J. Geophys. Res*, *102*(B3), 5005–5017.

Appendix A. Publications and/or Presentations Related to this Award

Bormann, J. M., W. C. Hammond, C. Kreemer, and G. Blewitt, 2012, Using GPS measurements of active crustal deformation to estimate slip rates on the Honey Lake/Warm Springs and Mohawk Valley fault systems, Northern Walker Lane, *Friends of the Pleistocene Pacific Cell Field Trip Guide Book, Neotectonics of the Lake Tahoe and Carson and Sierra Valleys*, September 13-16, 2012.

Hammond, W. C., C. Kreemer, G. Blewitt, and J. Bormann, 2012, GPS measurement of active crustal deformation of the Lake Tahoe basin and vicinity, *Friends of the Pleistocene Pacific Cell Field Trip Guide Book, Neotectonics of the Lake Tahoe and Carson and Sierra Valleys*, September 13-16, 2012.

Hammond, W.C., G. Blewitt, Z. Li, C. Kreemer, H.-P. Plag, 2012, Contemporary uplift of the Sierra Nevada, western United States, from GPS and InSAR measurements, *Geology, v. 40, p.* 667-670*,* doi:10.1130/G32968.1.

Wesnousky, S. G., J. Bormann, C. Kreemer, W. C. Hammond, and J. N. Brune, 2012, Neotectonics, geodesy, and seismic hazard in the Northern Walker Lane of Western North America: Thirty kilometers of crustal shear and no strike-slip?, *Earth and Planetary Science Letters*, *doi:10.1016/j.epsl.2012.02.018*.

Briggs, R.W. and Hammond, W.C., 2011, Evaluation of geodetic and geologic datasets in the Northern Walker Lane—Summary and recommendations of the Workshop: U.S. Geological Survey Open-File Report 2010–1282, 76 p.

Hammond, W.C., G. Blewitt, C. Kreemer, 2011, Block modeling of crustal deformation of the northern Walker Lane and Basin and Range from GPS velocities, *J. Geophys. Res., v. 116,* B04402, doi:10.1029/2010JB007817.

Kreemer, C. and W.C. Hammond, 2010, Geodetic constraints on the slip rate of the Mohawk Valley Fault Zone, California, Final Technical Report for NEHRP Award 08HQGR0027, April 2010.

Abstracts

Bormann, J. M., W. C. Hammond, C. Kreemer, and G. Blewitt, 2012, Active deformation in the Northern Walker Lane: A detailed geodetic study of the Mohawk Valley and Honey Lake/Warm Springs fault systems, *Eos Trans. AGU, Fall Meeting Abstract G22B-03*.

Bormann, J. M., W. C. Hammond, C. Kreemer, and G. Blewitt, 2012, Using GPS to measure slip rates on the Honey Lake/Warm Springs and Mohawk Valley fault systems, Northern Walker Lane, in *SCEC Annual Meeting*, edited, Palm Springs, CA.

Bormann, J., W.C. Hammond, C. Kreemer, 2011, Using EarthScope and MAGNET GPS to determine the slip rate on the Honey Lake Fault, northern Walker Lane, California, *EarthScope National Meeting*, Austin, TX, May 17-20, 2011.

Bormann, J., W.C. Hammond, C. Kreemer, G. Blewitt, 2011, GPS constraints on crustal deformation in the central Walker Lane and Sierra Nevada range front, *SCEC Annual Meeting*, Palm Springs, CA, Sept 11-14, 2011.

Bormann, J., W.C. Hammond, C. Kreemer, S. Wesnousky, G. Blewitt, 2011, Resolving the discrepancy between geodetic and geologic estimates of fault slip rates in the central Walker Lane: A block modeling approach, Abstract G53C-04, *Fall Meeting*, *AGU*, San Francisco, CA, 5-9 Dec, 2011.

Wesnousky, S., C. Kreemer, W.C. Hammond, J. Bormann, J.N. Brune, 2011, Neotectonics,

geodesy and seismic hazard in the Northern Walker Lane, Abstract S12A-02, *Fall Meeting, AGU*, San Francisco, CA, 5-9 Dec. [INVITED].

Bormann, J.L., W.C Hammond, C. Kreemer, G. Blewitt, S. Wesnousky, 2010, Crustal deformation of the central Walker Lane from GPS velocities: Block rotations and slip rates, Abstract T33A-2224, *Fall Meeting, AGU*, San Francisco, CA, 13-17 Dec, 2010.

Hammond, W.C., C. Kreemer, G. Blewitt, 2010, Using geodesy to reveal deformation partitioning and to probe the lower crust beneath the northern Walker Lane, *GSA Annual Meeting,* Session T151, Denver, CO, Oct. 31-Nov. 3, 2010 [INVITED].

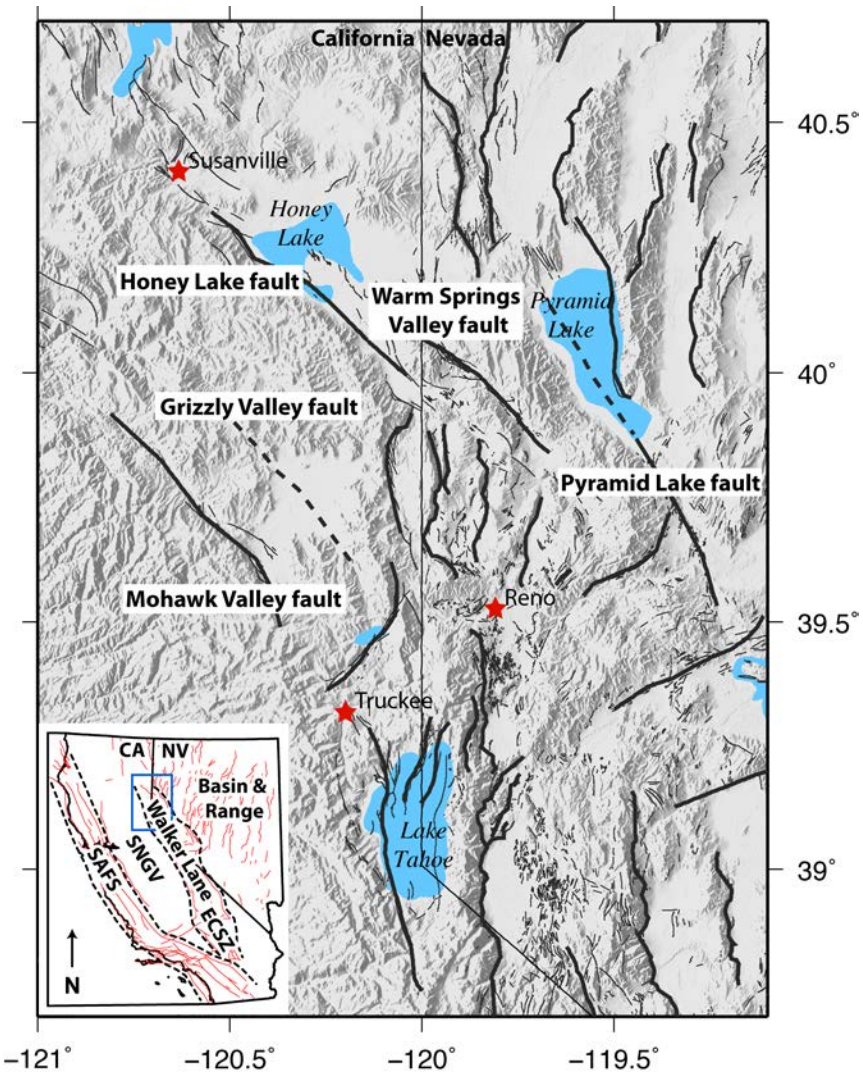

Figure 1. Regional map showing topography and location of faults in the Northern Walker Lane. Towns and cities are indicated by red stars. Inset shows location of region in relation to other elements of the Pacific/North America Plate boundary zone.

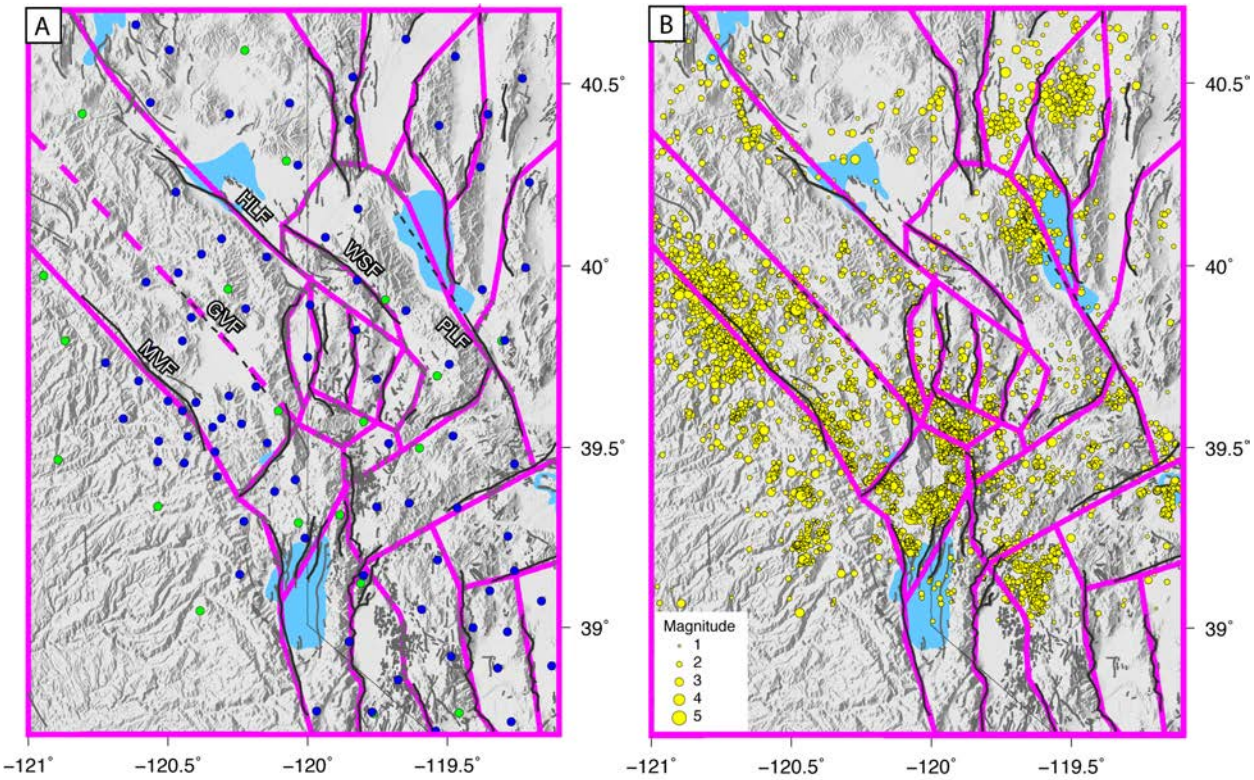

Figure 2. A) Location of GPS stations from the MAGNET (blue) and other continuous (green) stations. Block boundaries used for the deformation analysis are shown in the magenta lines. MVF - Mohawk Valley Fault, GVF Grizzly Valley Fault, HLF - Honey Lake Fault, WSF - Warm Springs Fault, PLF - Pyramid Lake Fault. B) Regional seismicity with yellow circle size indicating magnitude [*ANSS*, 2011].

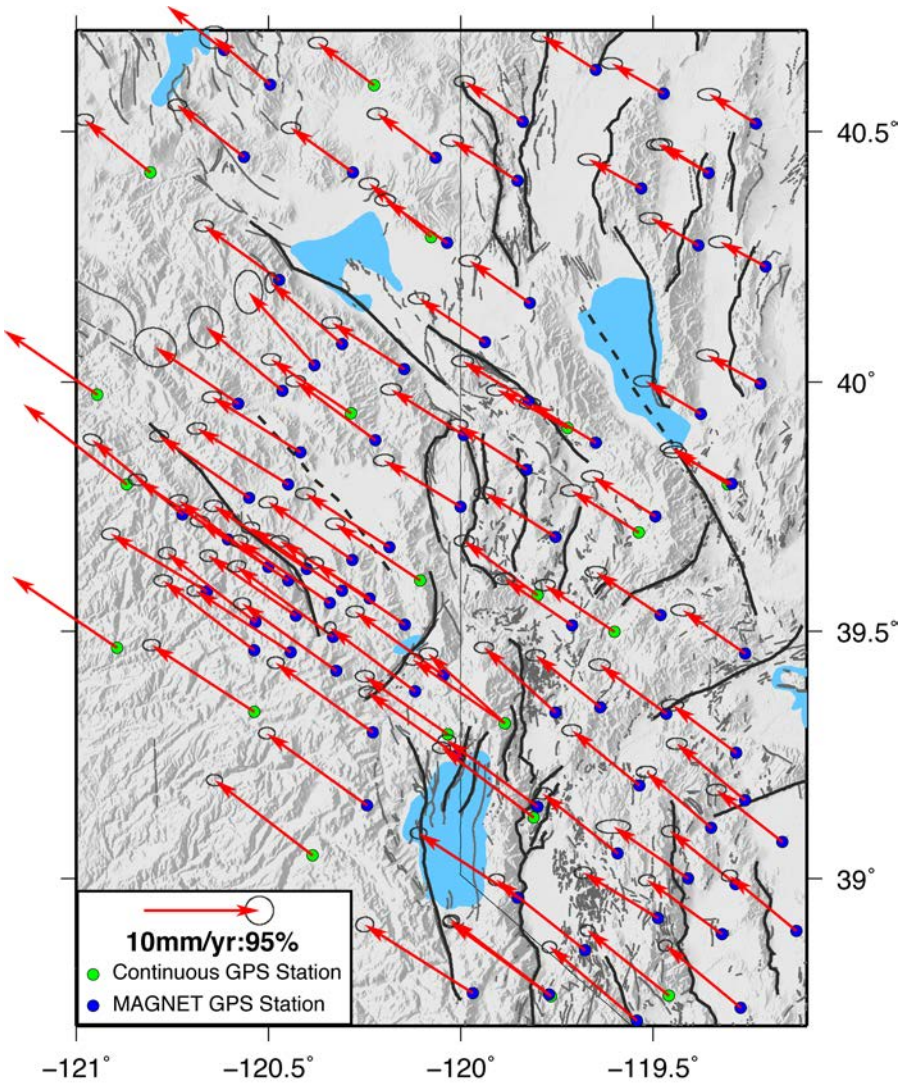

Figure 3A. GPS velocity in the NA12 North America reference frame.

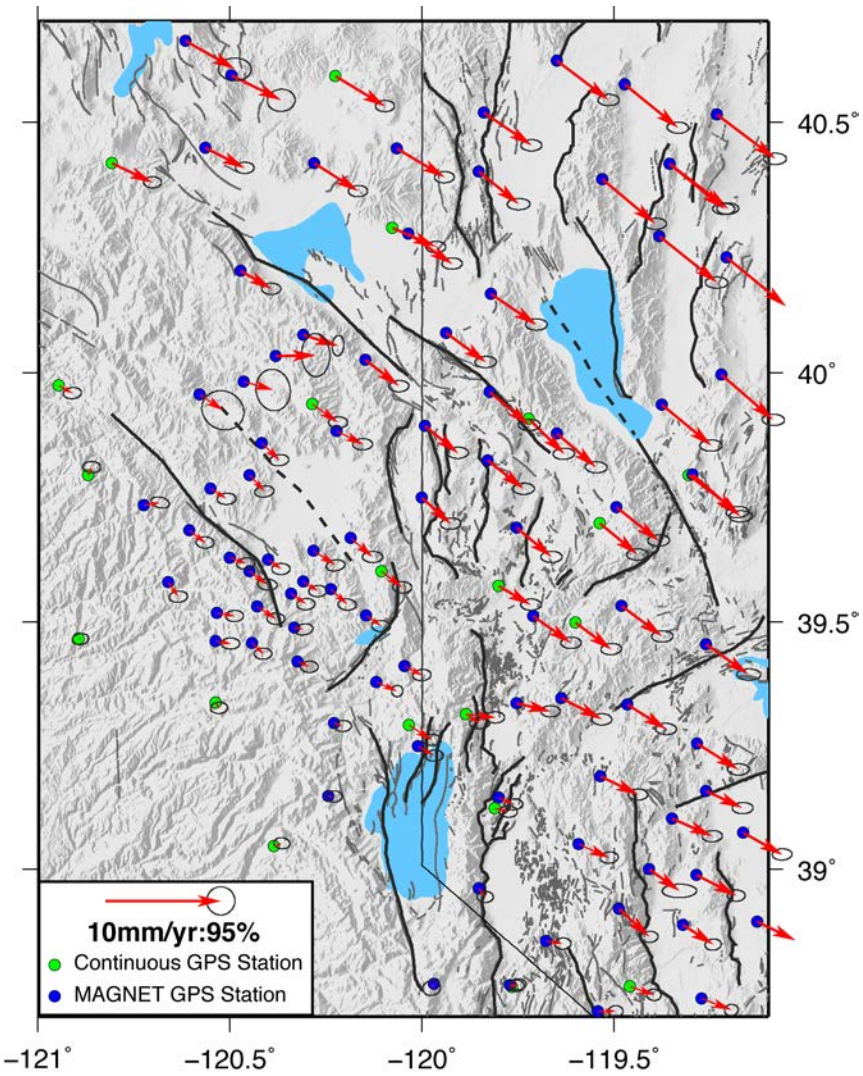

Figure 3B. Same as Figure 3A, but GPS velocity in presented in a Sierra Nevada/Great Valley fixed reference frame.

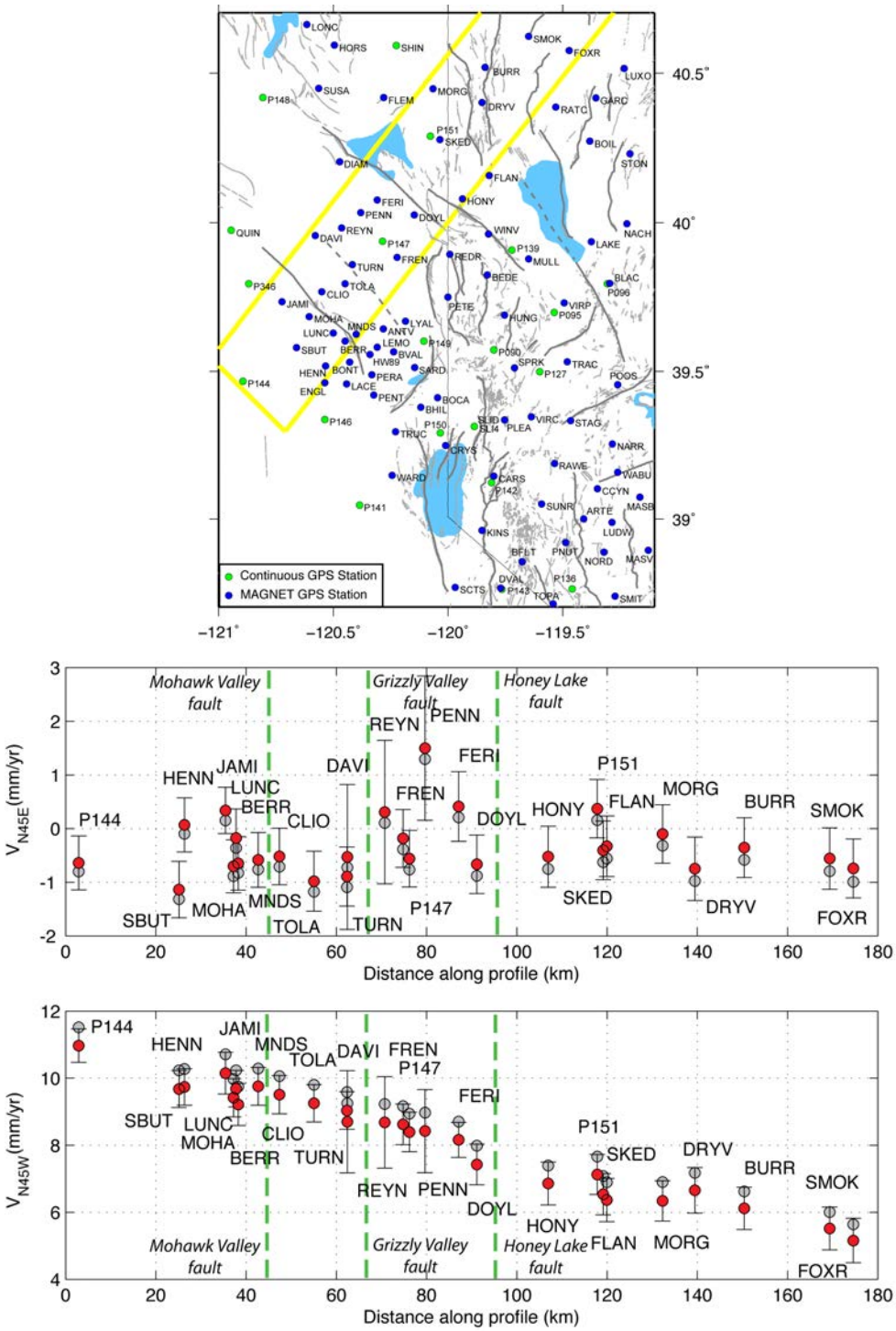

Figure 4. Top) Legend map showing location of GPS velocity profile extending from southwest of Mohawk Valley fault (near station P144) to northeast of the Honey Lake fault (near station SMOK). Middle) Velocity in N45˚E direction, parallel to profile, Bottom) velocity in N45˚W direction normal to profile. Gray circles are the observed rates, red circles with 2 sigma error bars are the rates corrected for the effects of viscoelastic postseismic relaxation from the Central Nevada Seismic Belt [*Hammond et al*., 2009].

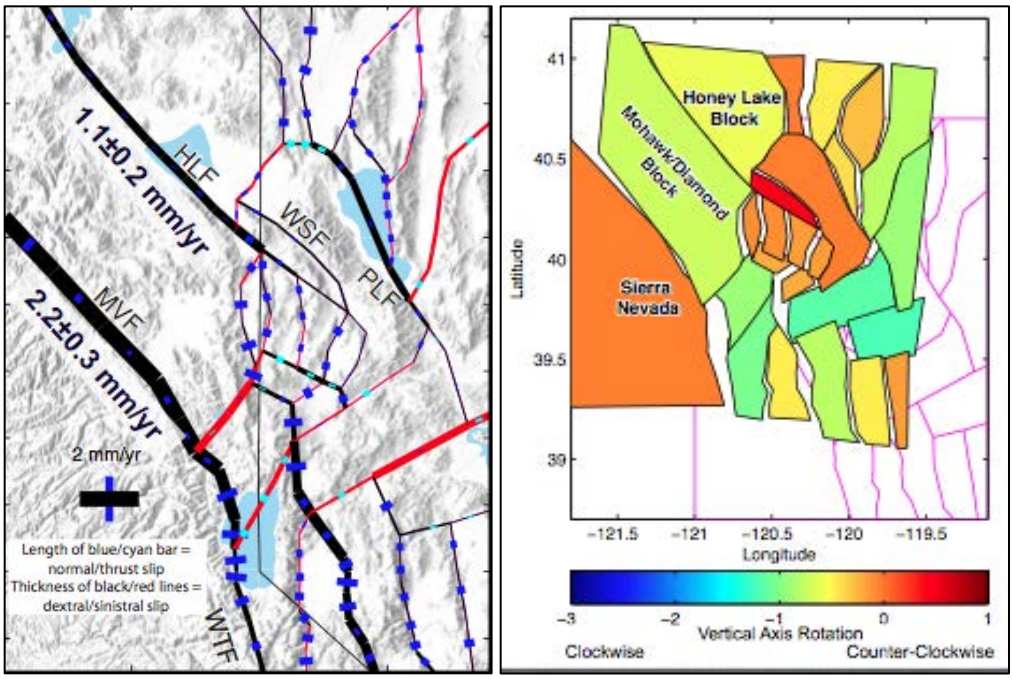

Figure 5. Left) Block model slip rates represented by thickness of black (red) line for dextral (sinistral) strike-slip and length of blue (cyan) bar for fault normal slip. Right) Block model rotation and translation rate represented by color with an exaggeration factor of 10^7 (10 million years of deformation). Color indicates vertical axis spin rate.

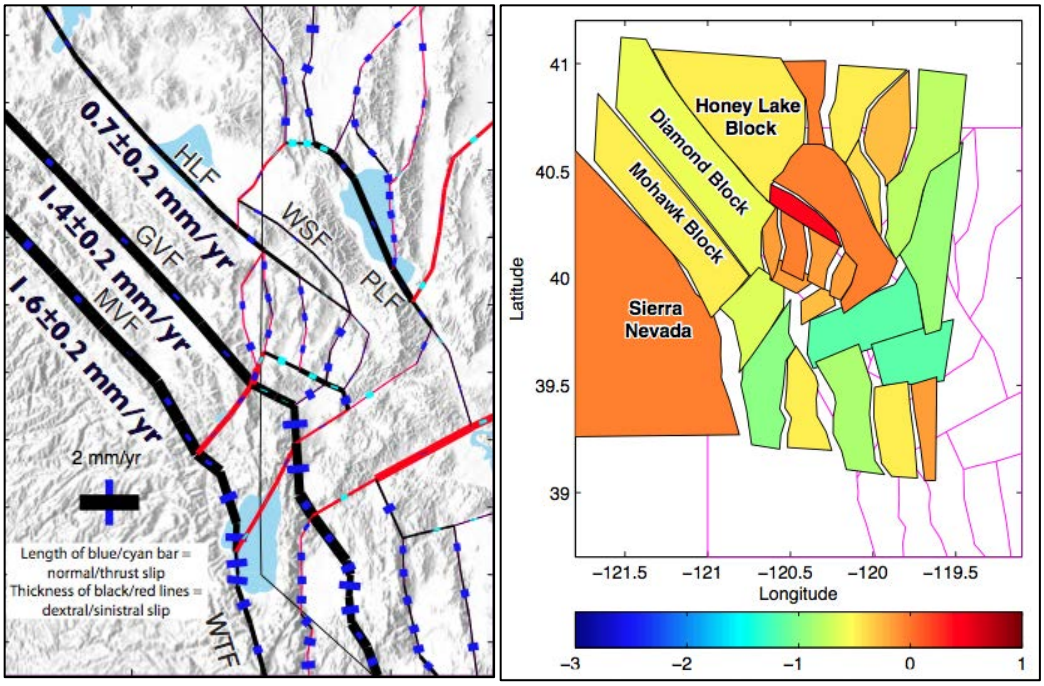

Figure 6. Same as Figure 5 except that both panels show the model where the Grizzly Valley fault has been included in the analysis. The Diamond Block and the Mohawk blocks are allowed to move separately.

Table 1. Slip rate estimates for faults considered in this study.

Method	Time Scale (ybp)	Site	Slip Rate (mm/yr)	Type	Reference
		Mohawk Valley fault zone			
Geologic	Holocene	Turner Creek (eastern fault strand)	0.3-0.5 minimum	dextral	Saywer et al., 2005
Geodetic	<10		2.9±0.2	dextral	Hammond et al., 2011
		Grizzly Valley fault zone			
Geologic	150,000		Quaternary active possibly Holocene active	dextral	Gold et al., 2012b
		Honey Lake fault zone			
Geologic	12,500-7000	Long Valley Creek-Site 1	1.1-2.6	dextral	Wills and Borchardt, 1993
Geologic	4670	Long Valley Creek-Site 1	1.7±0.6 minimum	dextral	Turner et al., 2008
Geologic	15,800-4,700	Long Valley Creek-Site 1	1.2-4.1	dextral	Gold et al., 2012a
Geologic	**15,800***-4,700	Long Valley Creek-Site 2	**2.3***-7.8	dextral	Gold et al., 2012a
Geologic	15,800-**4,700***	Long Valley Creek-Site 3	0.4-**1.4***	dextral	Gold et al., 2012a
Geodetic	<10		1.2±0.6	dextral	Hammond et al., 2011
		Warm Springs fault zone			
Geologic	15,800	Fort Sage Fan	0.2 maximum	dextral	Gold et al., 2013
Geologic	~50,000	Fort Sage Fan	$1.8^{+0.8}_{-0.8} - 2.4^{+1.2}_{-1.1}$	dextral	Gold et al., 2013
Geologic	300,000-50,000	Fort Sage Fan	0.3-2.2	dextral	dePolo, 2006
Geodetic	<10		1.0±0.6	dextral	Hammond et al., 2011

*Bold text indicated preferred ages and slip rates

Table 2. Parameters used in block modeling.

Type	Value	Unit
Locking depth (L)	15	km
Poisson's ratio (v)	0.25	-
Shear modulus (μ)	3×10^{10}	Pa s
Slip rate consistency (α)	10^{-6}	m yr^{-1}
Block centroid vertical axis rotation damping (β)	5×10^{-9}	rad yr^{-1}
Slip rate damping (Υ)	4×10^{-4}	m yr^{-1}